

Electronic structure and transport properties of TlInSe_2 and $\text{Tl}_{0.5}\text{Li}_{0.5}\text{InSe}_2$

A. Ghafari, K. Habicht

*Helmholtz-Zentrum Berlin für Materialien und Energie GmbH, Hahn-Meitner-Platz 1, 14109
Berlin, Germany*

Abstract

We report calculations of the electronic structure of thermoelectric ternary chalcogenide TlInSe_2 in the pressure range 0-30 GPa and the Li-substituted compound $\text{Tl}_{0.5}\text{Li}_{0.5}\text{InSe}_2$ using density functional theory. Moreover, with Boltzmann transport theory the electronic transport properties of these compounds are investigated at the optimal p-doping level for a maximized power factor. We follow two possible band engineering routes by applying pressure and elemental substitution with Li to investigate a possible enhancement of the electronic properties for thermoelectric applications. Our study employs several exchange-correlation functionals including the spin-orbit interaction as well as the B3LYP hybrid functional. The band gap in TlInSe_2 obtained by using the Tran-Blaha modified Becke-Johnson functional is in good agreement with experimental data. We find a direct band gap for TlInSe_2 at the M-point and a slightly larger energy gap at the Z-point. The spin-orbit (SO) splitting is extracted from the calculated electronic band structure. When applying pressure to TlInSe_2 the Seebeck coefficient strongly decreases and band crossing results in metallic properties above 20 GPa. In contrast to TlInSe_2 , an indirect band gap is found for $\text{Tl}_{0.5}\text{Li}_{0.5}\text{InSe}_2$ with the valence band maximum located at an off-symmetry point along the M-X direction and the conduction band minimum located at an off-symmetry point along the X-P direction. In contrast to TlInSe_2 at ambient pressure, taking the SO coupling into account for $\text{Tl}_{0.5}\text{Li}_{0.5}\text{InSe}_2$ and TlInSe_2 at 20 GPa is necessary as it markedly changes the transport properties. Optimally doped p-type TlInSe_2 at ambient pressure has the most favorable electronic band structure for thermoelectric applications superior to both, optimally doped p-type TlInSe_2 under pressure and optimally doped p-type $\text{Tl}_{0.5}\text{Li}_{0.5}\text{InSe}_2$.

I. Introduction

Research on thermoelectric (TE) materials is a topic of renewed interest in condensed matter physics driven by the need for sustainable electrical power generation. In these materials the Seebeck effect allows for the direct conversion of thermal energy into electrical energy. Thermoelectricity thus attracts great attention due to its potential for harvesting enormous amounts of waste heat [1, 2]. Prior to widespread industrial applications, however, it is desirable to significantly increase the energy conversion efficiency. The efficiency of TE materials is determined by the dimensionless figure of merit $ZT = (S^2\sigma/\kappa)T$, where T is the temperature and S , σ and κ are the Seebeck coefficient, the electrical conductivity and the total thermal conductivity provided by electrons and phonons, respectively. Since these transport properties are strongly interrelated, enhancing the figure of merit towards technologically useful device efficiencies provides a formidable challenge. Among the different optimization strategies which have been developed, dimensional confinement has been identified as an efficient mechanism to reduce the lattice (phonon) thermal conductivity by the increase of the phonon scattering rate [3]. Confinement effects in the electronic system, e.g. in superlattices and quantum wells, have been shown to lead to an enhanced Seebeck coefficient by the increase of the electronic density of states (DOS) [4] thereby increasing the power factor $PF = S^2\sigma$.

Here we investigate the electronic properties of ternary chalcogenide TlInSe_2 which is an example of a crystalline quasi-one-dimensional (1D) phonon material and has been reported to exhibit a large Seebeck coefficient exceeding $10^6 \mu\text{V/K}$ at temperatures $T < 450 \text{ K}$ [5]. Despite the debatable relevance of the compound for direct technological applications due to the toxicity of Tl, TlInSe_2 may be regarded as a model system which exhibits a quasi-1D phonon structure. Due to its moderate number of atoms in the crystallographic unit cell this compound is amenable to theoretical modelling by density functional theory (DFT) with moderate computational effort. The crystalline

substructure of TlInSe_2 consists of chains of trivalent In atoms which have covalent bonds to Se atoms arranged along the crystallographic c-axis [6]. A weaker ionic bond of monovalent octahedrally coordinated Tl atoms provides a weak connection of these chains to each other. These structural properties put TlInSe_2 into the class of intrinsically nanoscaled materials with quasi-1D phonon properties which are expected to have favorable consequences for the lattice dynamics limiting the propagation of phonons and thereby decreasing the thermal conductivity [7]. TlInSe_2 is thus believed to hold the potential for a very large figure of merit $ZT > 2$ at $T < 500$ K [5] exceeding the ZT of PbTe or PbSe with ZT -values of ~ 1.8 [8, 9]. The study of the phonon properties of TlInSe_2 is, however, beyond the scope of the present work. Instead we focus on the investigation of the electronic structure of undoped TlInSe_2 and the transport properties of p-doped TlInSe_2 assuming the validity of the rigid-band model. Besides the quasi-1D phonon character of TlInSe_2 , structural phase transitions at 185 K and 130 K have been reported [10] which call for angle-resolved photoemission spectroscopy (ARPES) experiments investigating a possible electronic mechanism related to the structural phase transitions of TlInSe_2 . Prior to the experiment numerical electronic structure data is required, motivating our DFT study of TlInSe_2 .

The first electronic structure calculation of TlInSe_2 reported by Gashimzade and Orudzhev [11] is based on the empirical pseudopotential method. Later calculations were based on the pseudopotential method allowing for non-locality of the ionic pseudopotential [12]. Today it is well known that the local density approximation (LDA) [13] and the generalized gradient approximation (GGA) functionals underestimate the size of the band gap of semiconductors [14, 15]. Therefore in our study of the electronic structure of TlInSe_2 we have used the Tran-Blaha modified Becke-Johnson (TB-mBJ) functional [16, 17] and the B3LYP hybrid functional [18] in addition to the Perdew-Burke-Ernzerhof (PBE) functional [19] to compare with. Since TlInSe_2 contains heavy elements including the spin-orbit (SO) coupling is a prerequisite for a correct description of its

electronic structure. In contrast to previous work [11, 12], our calculations have been performed with and without SO interaction. This allows for a direct comparison with experimental data and thus allows for an assessment of the impact of SO coupling on the electrical transport properties.

Our main motivation to study the evolution of electronic properties with hydrostatic pressure is to evaluate whether band-gap tuning by applied pressure, as known from other thermoelectric materials [20, 21], is a promising optimization strategy for TlInSe₂. We discuss the modifications of the bandstructure with pressure and their impact on the transport properties. Experimentally it has been demonstrated that the resistivity of TlInSe₂ decreases continuously with increasing hydrostatic pressure [22]. However, the experimental data was limited to a maximum accessible pressure of 7 GPa where the system is still in the semiconducting state. Our theoretical study investigates the electronic structure of crystalline TlInSe₂ under hydrostatic pressure up to 30 GPa thus we are able to identify the transition pressure to the metallic state just above 20 GPa.

Elemental substitution provides an alternative route to modify the electronic band structure significantly which motivates our investigation of the electronic structure and the transport properties of the Li-substituted compound Tl_{0.5}Li_{0.5}InSe₂. Li-substitution is chosen to study the effect of isovalent substitution of Tl without affecting the charge carrier concentration by doping. Both Li-Se and Tl-Se possess a strong ionic bonding character [23] but changes in the electronic structure can be expected due to the significantly different band gap of LiInSe₂. The latter compound is known to be a wide-band gap semiconductor with a gap energy $E_{\text{gap}}=2.85$ eV [23] as opposed to TlInSe₂ where $E_{\text{gap}}=1.1-1.4$ eV [24-25]. Although the phase stability of the hypothetical compound Tl_{0.5}Li_{0.5}InSe₂ is yet to be demonstrated the successful synthesis of large single crystals of LiInSe₂ [26, 27] and thin films of Cu_{0.5}Li_{0.5}InSe₂ [28] suggests that thermodynamic stability of

$\text{Tl}_{0.5}\text{Li}_{0.5}\text{InSe}_2$ is plausible. Our DFT calculations allow us to evaluate the electronic density of states and transport properties for 50% Li-substitution where a rigid-band model is inappropriate.

This article is organized as follows. After a short description of the methods used in section II, we report the results of DFT calculations for the electronic band structure of TlInSe_2 using different functionals and with and without the SO interaction in section III.A. The orbital character of the electronic bands is discussed in detail in section III.B. In section III.C the modification of the electronic structure of TlInSe_2 under hydrostatic pressure up to 30 GPa is investigated. The electronic structure as obtained for $\text{Tl}_{0.5}\text{Li}_{0.5}\text{InSe}_2$ is presented in section III.D. Finally, in section III.E transport properties calculated with Boltzmann transport theory for p-doped TlInSe_2 and p-doped $\text{Tl}_{0.5}\text{Li}_{0.5}\text{InSe}_2$ at ambient pressure as well as for p-doped TlInSe_2 under a hydrostatic pressure of 20 GPa are discussed. Section IV concludes the article with a summary of the results.

II. METHODS

The DFT calculations were performed with the Wien2k code [29] which is based on the full-potential linearized augmented plane-wave method (FP-LAPW). We have used the body-centered tetragonal crystal structure with space group I4/mcm (Nr.140) for TlInSe_2 and the experimental room temperature lattice parameters of $a=8.075 \text{ \AA}$ and $c=6.847 \text{ \AA}$ [6]. The atomic positions for Se, In, and Tl in crystallographic notation are (0.18 0.68 0.00), (0.00 0.50 0.25) and (0.00 0.00 0.25), respectively. Using the experimental lattice parameters of TlInSe_2 , convergence tests for the number N_k of k-points in the Brillouin zone (BZ), the magnitude of the largest vector in the charge density Fourier expansion G_{max} , and the smallest muffin-tin radius R_{MT} times the largest wavevector k_{max} for the plane-wave expansion of the wave function were performed. We used values of $N_k=600$, $G_{\text{max}}=14 \text{ (a.u.)}^{-1}$, and $R_{\text{MT}} k_{\text{max}}=8.5$. The volume of the crystallographic unit cell was only optimized ($a_{\text{T}}=7.9585 \text{ \AA}$ and $c_{\text{T}}=6.7482 \text{ \AA}$ for TlInSe_2) with the Wu and Cohen (WC) functional [30] by varying the volume with a constant a:b:c ratio as implemented in the Wien2k code. The

optimization of the structure has not been performed with any other functional such as the B3LYP hybrid functional. The structure was fully relaxed until the forces on each atom reached less than 0.001 Ryd/Bohr. The same method has been used for the Li-substituted compound $\text{Tl}_{0.5}\text{Li}_{0.5}\text{InSe}_2$ assuming the same tetragonal crystal structure, which gives lattice constants $a_1=7.8802 \text{ \AA}$ and $c_1=6.6818 \text{ \AA}$. The calculations of the electronic structure have been performed with the PBE and TB-mBJ exchange-correlation functionals and the B3LYP hybrid functional in order to find the best match with experimental data for the band gap and the SO splitting.

The transport calculations were based on Boltzmann transport theory with the constant relaxation time approximation using the BoltzTraP code [31] with a dense mesh of 60000 k-points in the BZ to achieve convergence. Within this approximation the Seebeck coefficient is independent of the electronic relaxation time τ . However, the electrical conductivity σ , the power factor PF and the electronic thermal conductivity κ_e can only be calculated as σ/τ , $\text{PF}/\tau= S^2\sigma/\tau$ and κ_e/τ and further assumptions about τ have to be made. This is discussed in detail in section III.E which focusses on the transport properties of TlInSe_2 and $\text{Tl}_{0.5}\text{Li}_{0.5}\text{InSe}_2$.

III. RESULTS AND DISCUSSION

A. Electronic Band Structure of TlInSe_2

As we are interested in the temperature-dependent transport properties of TlInSe_2 and in view of the fact that it is notoriously difficult to precisely predict band gaps from DFT calculations our comparison of the electronic band structures obtained with different functionals first of all focusses on the size of the band gap (Table 1). All functionals yield a direct band gap at the M-point. A second VBM and a second CBM are located at the Z-point. This maximum (minimum) is only slightly lower (higher) in energy, typically tens of meV, as compared to the VBM (CBM). Referring to the DFT calculation with the TB-mBJ exchange-correlation functional, for example, the energy

of the second VBM at the Z-point is only 40 meV lower in energy than the VBM at the M-point. In Table 1 we also give the energy corresponding to the indirect gap with the VBM at the M-point and the CBM at the Z-point. These values are systematically larger than the direct band gap but the difference is only on the order of 0.1 eV.

Substantial differences are obtained for the absolute magnitude of the band gap. As expected from previous work on other semiconductors [16, 32-34], the PBE functional underestimates the magnitude of the band gap in TlInSe₂ in contrast to the B3LYP hybrid functional and the TB-mBJ exchange-correlation functional. FIG. 1a and b shows the electronic band structure calculated with these functionals. Using the B3LYP hybrid functional the VBM at the Γ -point and N-point are located below the Fermi level about 1.26 eV and 1.12 eV, respectively. Corresponding values for the TB-mBJ exchange-correlation functional are 1.38 eV and 1.08 eV, respectively. Overall, the dispersions of the valence bands obtained with all functionals used in this work show a similar structure.

The magnitudes of the direct and indirect band gaps of TlInSe₂ calculated with the B3LYP hybrid functional and the TB-mBJ exchange-correlation functional are comparable to experimental data obtained by optical absorption spectroscopy. Experimental values have been reported in literature to be 1.07 eV (1.35 eV) [24] and 1.21 eV (1.27 eV) [25], for the indirect (direct) gaps. Moreover, a band gap of 1.12 eV has been obtained by electrical conductivity measurements [22]. Using the TB-mBJ exchange-correlation functional shows best agreement with the experimental data. Given the fact that the absolute energy differences between VBM/CBM at the M-point and the extrema in the VB at the Z-point are small, the discrepancy between DFT which predicts a direct band gap at the M-point and the experiment which reports an indirect band gap across M-Z is not surprising.

Besides the similar accuracy for the band gap obtained with the two functionals the TB-mBJ exchange-correlation functional offers the advantage of being less expensive than the B3LYP hybrid functional. We have therefore restricted the evaluation of the density of states and our investigations of hydrostatic pressure and Li-substitution to DFT calculations exclusively based on the TB-mBJ exchange-correlation functional.

Taking the SO coupling into account, the conduction band (CB) is systematically shifted down in energy relative to the valence band (VB) thus reducing the size of the band gap by ~ 0.2 eV (see Table 1). At the same time the degeneracy of some VBs is removed. Bands which are significantly affected by the SO splitting are marked in blue color in FIG. 1c. Since the modification only involves bands deep in the valence band, i.e. well below the VBM, the SO interaction is expected to have little impact on the thermoelectric properties even for a p-type semiconductor. Our calculations reveal that at the Γ -, M-, and Z-points the SO splittings are $\Delta_{\text{SO-}\Gamma}=354$ meV, $\Delta_{\text{SO-M}}=170$ meV, and $\Delta_{\text{SO-Z}}=141$ meV based on the TB-mBJ exchange-correlation functional.

At the M-point we have determined the effective masses of charge carriers in the VBM (holes) and in the CBM (electrons) along the crystallographic a, b, and c directions by fitting the conduction and valence bands to parabolas in the wavevector interval $\pm 0.02 \text{ \AA}^{-1}$. The corresponding results are presented in Table 2. Due to the tetragonal crystal symmetry the effective masses along the a- and b-directions are equal. They are identical to the effective mass along the Γ -M direction. The larger difference of the VB effective masses and the smaller difference of the CB effective masses between the a- and c-directions suggest that the anisotropy of the electronic properties is more pronounced for p-doped TlInSe₂. The maximum effective mass $m_c^*=1.76m_0$ for charge carriers in the VB is obtained along the c-direction contributing to a lowering of the electrical conductivity along c. Besides possible anisotropic scattering rates this is in accordance with the experimental

finding $\sigma_c < \sigma_b$, where $\sigma_{b,c}$ are the electrical conductivities along the crystallographic b and c axes. Zeier *et al.* [35] have emphasized that the peak figure of merit ZT at optimized charge carrier concentration depends on the thermoelectric quality factor B. Applying deformation potential theory [36], the quality factor B can be shown to be proportional to the valley degeneracy N_V and inversely proportional to the inertial effective mass $m_I^* = 3/(2/m_a^* + 1/m_c^*)$. Large valley degeneracy and low inertial effective mass are thus beneficial for the thermoelectric properties. For fixed carrier concentration a high Seebeck coefficient is due to a large density of states effective mass $m_{DOS}^* = N_V (m_a^* m_c^*)^{1/3}$. At the M-point $N_V = 1$, since each of the 4 M-points at the Brillouin zone boundary is shared with 4 neighboring unit cells of the reciprocal lattice. For p-doped TlInSe₂ a lower inertial effective mass $m_{I,VBM}^* = 0.43m_0$ coincides with a larger density of states effective mass $m_{DOS,VBM}^* = 0.55 m_0$, enhancing both, quality factor and Seebeck coefficient. Note that this is not the case at the CBM, where $m_{I,CBM}^* = 0.54m_0$ and $m_{DOS,CBM}^* = 0.55 m_0$. Finally, we note that the effective mass for holes at the Γ -point in the Γ -M direction is $0.49m_0$.

B. Density of States and Orbital Character Analysis

FIG. 1a-g shows the electronic band structure and the total and partial density of states (DOS). Three groups of bands are easily identified. The first group of bands, lowest in energy and located around $E = -10.2$ eV is dominated by a strong contribution of Tl-d states (FIG. 1g) accompanied with only a small contribution of Se-s-states (FIG. 1e) and In-d-states (FIG. 1f). The SO interaction apparently affects the position of the Tl-d-states with respect to the Fermi level which we have chosen to coincide with the VBM. With the SO interaction these states are shifted about 850 meV closer to the VBM (cf. FIGS. 1b and 1c). These states are irrelevant for the transport properties but useful for comparison with ARPES data. The second group of bands ranges from about -7 eV to the Fermi level. This is the valence band which is mainly composed of Se-p-states and Tl-s-states. However, a small contribution of In-p and In-d states is also present (see FIGS 1e-g). Band character

analysis reveals that the VB maxima at the M- and Z-points of the BZ have a strong contribution from Se- p_y and Tl-s states dominating transport in p-doped TlInSe₂. The total DOS between -7 eV and the Fermi energy exhibits two peaked structures at -2 eV and -5.5 eV. This agrees well with experimental data by Kilday et al. [37] who observed a pronounced peak 1.5 eV below the Fermi level and weaker peak 5.5 eV below the Fermi level by photoemission spectroscopy. These peaks were attributed to the Se-4p states and the Tl-6s state, respectively. Our DFT calculation reveals that for the second peak at -5.5 eV besides Tl-6s, the contributions of Se-s, Se-p and In-s orbitals are also significant (FIG. 1e and f). The third group of bands forms the conduction band shown from 1 eV to 6 eV. This is a mixture of several orbitals. Transport in n-doped TlInSe₂ is dominated by contributions from Tl-p-orbitals, Se-p-orbitals and the In-s-orbital since those states contribute significantly to the lowest conduction band.

C. Electronic Band Structure of TlInSe₂ under Hydrostatic Pressure

A successful strategy to enhance TE properties in particular at lower temperatures is the application of pressure [20, 21]. Pressure changes the bonding properties and thus reflects in the band structure and ultimately in the Seebeck coefficient S and in the electrical conductivity σ . Given the proximity of the band gap energies of TlInSe₂ at the M-point and the Z-point in the BZ, one might speculate that moderate pressure may increase the DOS at the VBM and the CBM beneficial for the TE performance. In addition, a decrease of the band gap changes the charge carrier concentration at fixed temperature. In this section we investigate the evolution of the band structure of TlInSe₂ with hydrostatic pressure in the range 0-30 GPa. We note that applying and controlling hydrostatic pressures as high as 30 GPa to TE materials is exceedingly difficult for the experiment [38]. Previous experimental investigations [22] have been limited to a maximum pressure of 7 GPa. Murnaghan's equation of state [39] has been used in order to obtain the volume of crystal structure

at elevated pressures while the bulk modulus and the pressure derivative of the bulk modulus have been obtained by fitting Murnaghan's equation of state to the total energy as a function of the volume of the unit cell at a different pressure. The lattice parameters $a_T= 7.8637 \text{ \AA}$ and $c_T= 6.6678 \text{ \AA}$; $a_T= 7.7487 \text{ \AA}$ and $c_T= 6.5703 \text{ \AA}$; $a_T= 7.6021 \text{ \AA}$ and $c_T= 6.4460 \text{ \AA}$; $a_T= 7.4898 \text{ \AA}$ and $c_T= 6.3508 \text{ \AA}$; $a_T= 7.3991 \text{ \AA}$ and $c_T= 6.2739 \text{ \AA}$; $a_T= 7.3231 \text{ \AA}$ and $c_T= 6.2094 \text{ \AA}$; $a_T= 7.2578 \text{ \AA}$ and $c_T= 6.1540 \text{ \AA}$ have been calculated for pressures of 2 GPa, 5 GPa, 10 GPa, 15 GPa, 20 GPa, 25 GPa, 30 GPa, respectively. The electronic transport properties of TlInSe₂ under pressure are discussed in detail in section III.E.

The results of our calculations which have been performed using the TB-mBJ functional with SO and without SO (WSO) interaction are presented in FIG. 2 and Table 1. By increasing the pressure from 0 to 30 GPa the VB width continuously increases from 6.71 eV to 8.99 eV (SO). Simultaneously, the CB and thus the DOS shift to lower energies (see FIG. 2c). Hence, the VBM and CBM approach each other thus reducing the magnitude of the band gap (FIG. 2d and e). Qualitatively this is in accord with a simple tight-binding model where the transfer integrals in the crystal Hamiltonian give a direct measure of the bandwidth. As the equilibrium distances between atoms are reduced with increasing pressure the transfer integrals get larger thus leading to an increased bandwidth.

Our calculations with the SO coupling show that there is still a minimal, but finite band gap at the M-point (0.02 eV) at 20 GPa whereas at 25 GPa TlInSe₂ has already undergone the semiconductor-metal transition. The VB and the CB clearly cross each other at pressures above 20 GPa (FIG. 2e). The local VBM at the Z-point stays below the VBM at the M-point throughout the semiconducting phase, so that a band alignment is not achieved by applying hydrostatic pressure to TlInSe₂. The gap at the Z-point remains finite at all pressures up to 30 GPa but at 25 GPa the band which approaches

the maximum at the Z-point from the Γ -Z direction has crossed the Fermi level (FIG. 2i) thus increasing phase space for charge carrier scattering. FIG. 2f (FIG. 2g) shows a magnified view of the dispersion of the VBM (CBM) at the M-point. Note that in order to facilitate comparison of the curvatures of the CBM at different pressures the dispersion at each pressure was shifted to the same reference energy. The wavevector axes in FIG. 2, panels f and g are chosen to coincide with the Γ -M-X direction thus effectively corresponding to the crystallographic (110) and (100) directions. Increasing the pressure from zero to 30 GPa leads to an increase of the curvature of the dispersion along the Γ -M direction so that the effective mass m_a^* of holes (electrons) is decreased. Again the simple tight-binding model can be invoked for a qualitative explanation: The effective masses are inversely proportional to the transfer integrals and thus decrease with increasing pressure. The effect, although beneficial for the quality factor B, is rather small so that the thermoelectric properties will be dominated by changes in the electrical conductivity due to the closure of the band gap with pressure.

The band structure of TlInSe₂ around the high symmetry directions of the BZ at 20 GPa just below the semiconductor-metal transition is shown in FIG. 2a. The SO splitting of bands (shown in blue color) remains at energy levels clearly below the VBM, i.e. deep inside the VB, for all pressures. Apart from the marked effect of reducing the bandgap, the presence of the SO coupling will thus not affect the transport properties. This statement applies also in the pressure regime where TlInSe₂ is already in the metallic phase. However, inside the VB significant changes in the magnitude of the SO splitting at the Γ -, M-, and Z- points of the BZ are induced by hydrostatic pressure (Table 1). In contrast to the behavior of the bandwidth, the SO splitting at the M-point decreases continuously from 170 meV at ambient pressure to 12 meV at 20 GPa. At larger pressures it increases again to 217 meV at 30 GPa thus reflecting a pressure-induced crossing of the SO-split bands. Since the presence of the SO interaction noticeably reduces the band gap the transition pressure when TlInSe₂

enters the metallic phase strongly depends on whether the SO interaction is considered or not. In the absence of the SO interaction no semiconductor-metal transition is induced up to 30 GPa (FIG. 2d).

D. Electronic Band Structure of Li-Substituted $\text{Tl}_{0.5}\text{Li}_{0.5}\text{InSe}_2$

Heavy doping or substitution of atoms provides an alternative route to manipulate the band structure. Even if the lattice symmetry remains unchanged substitution alters the band structure and redistributes the weight of the electronic states in both, the VB and the CB, thereby affecting the transport properties. In our DFT study we have investigated the electronic properties of $\text{Tl}_{0.5}\text{Li}_{0.5}\text{InSe}_2$ where 50% of the Tl-atoms are substituted by Li-atoms retaining the tetragonal crystal structure with a unit cell and atom positions as shown in FIG. 3. In contrast to hydrostatic pressure, Li-substitution is expected to increase the band gap. This is because LiInSe_2 is known to be a wide-band gap semiconductor with a gap energy $E_{\text{gap}} = 2.85$ eV [23, 40] much larger than the band gap of TlInSe_2 . Since both, Li-Se and Tl-Se possess a strong ionic bonding character [23] our choice of Li-substitution allows to study the effect of isovalent substitution of Tl without affecting the charge carrier concentration by concomitant doping. Although the complete phase diagram of $\text{Tl}_{0.5}\text{Li}_{0.5}\text{InSe}_2$ is not known and the phase stability of the hypothetical compound $\text{Tl}_{0.5}\text{Li}_{0.5}\text{InSe}_2$ against competing phases remains to be demonstrated experimentally, the successful synthesis of large single crystals of LiInSe_2 [26, 27] and thin films of $\text{Cu}_{0.5}\text{Li}_{0.5}\text{InSe}_2$ [28] suggests that the thermodynamic stability of $\text{Tl}_{0.5}\text{Li}_{0.5}\text{InSe}_2$ is plausible. Our calculated formation energy per atom of TlInSe_2 and $\text{Tl}_{0.5}\text{Li}_{0.5}\text{InSe}_2$ are -0.398 eV and -0.475 eV, respectively.

The effect of Li-substitution on the electronic structure was investigated again using the TB-mBJ exchange-correlation functional (FIG. 3 a and b). Apart from the important details discussed below, the gross features of the band structure do not depend on whether the SO interaction is considered or not. Compared to TlInSe_2 the band gap is significantly increased as expected. The band gap has

an absolute value of ~ 2.1 eV which is roughly the average of the band gaps of TlInSe_2 and LiInSe_2 . $\text{Tl}_{0.5}\text{Li}_{0.5}\text{InSe}_2$ is found to have an indirect band gap with the CBM located at $k_{\text{CBM1}} = (0.18, 0.18, 0.13)$ $1/\text{\AA}$ along the X-P direction. Moreover, three almost degenerate VBM, which are within an energy interval of 0.02 eV are located at $k_{\text{VBM1}} = (0.00, 0.37, 0.00)$ $1/\text{\AA}$ along the Γ -M direction, at $k_{\text{VBM2}} = (0.04, 0.36, 0.00)$ $1/\text{\AA}$ along the M-X direction and at the Z-point. In fact the dispersion between the two maxima at k_{VBM1} and k_{VBM2} is almost negligible (less than 0.02 meV) giving rise to an enhanced DOS in this region of the BZ but also a larger effective mass for the charge carriers. Furthermore, the local maximum at k_{VBM1} is located deep inside the BZ which effectively increases the valley degeneracy N_V for this particular maximum. The cumulative effect of these properties of the band structure leads to a modified power factor of p-doped $\text{Tl}_{0.5}\text{Li}_{0.5}\text{InSe}_2$ as shown in section III.E. Besides the CBM at k_{CBM1} two additional local minima are present which are located at the Γ -point and a second one located along the Γ -Z direction. However, their energy difference relative to the global CBM at k_{CBM1} is more than 100 meV.

FIG. 3c shows that in the Li-substituted compound the DOS of the VB is mainly composed of Se-states. A small contribution of Lithium-s and p states at the VB is also observed (FIG. 3d). A direct comparison of the DOS of TlInSe_2 with the DOS of $\text{Tl}_{0.5}\text{Li}_{0.5}\text{InSe}_2$ is depicted in FIG. 3k. Close to the Fermi level the DOS in the VB is increased by Li-substitution whereas the DOS in the CB is decreased upon Li-substitution. Thus for hole-doping (p-type semiconductor) the charge carrier concentration at constant temperature and consequently the electrical conductivity increase. The first peaks below the Fermi level which are located at -381 meV and -1.15 eV for the Li-substituted and the non-substituted crystals, respectively, are associated with a DOS of 8.16 states/eV and 4.45 states/eV. In addition, we note that the dispersion of the VBM is modified such that the effective mass of electrons is increased in the Li-substituted crystal leading to a reduced mobility. However, the charge carrier density increase dominates leading to an overall increase of the electrical

conductivity. Simultaneously, the DOS in the CB for undoped TlInSe₂ is rigidly shifted to higher energies (FIG. 3k). The increase in gap size counteracts the change of DOS. Thus the total effect on the relevant thermoelectric properties, namely the electrical conductivity and the Seebeck coefficient can only be inferred by a detailed quantitative analysis (see section III.E).

Finally, we comment on the SO splitting in Tl_{0.5}Li_{0.5}InSe₂. In contrast to TlInSe₂ where the SO splitting is only noticeable for a few bands deep inside the VB, the SO interaction in Tl_{0.5}Li_{0.5}InSe₂ does affect many electronic bands. In particular, differences occur close to the CBM and the VBM. FIG. 3e-j show a zoom into the dispersion of the VB and CB close to the Fermi level at the M- and Z-points as well as along the X-P direction of the BZ demonstrating the SO splitting of bands. Besides the absolute CBM at (0.18, 0.18, 0.13) 1/Å along the X-P direction two local minima at the Γ -point and along the Γ -Z direction are also observed which are 177 meV (256 meV) and 112 meV (196 meV) higher in energy for calculations WSO (with SO) interaction. Here, the SO interaction induces significant changes on the order of ~80 meV. The calculation with SO interaction reveals a splitting of the CBM at the N-, P- and Z-points of the BZ which are 57 meV, 118 meV, and 151 meV, respectively. The maximum size of the SO splitting at the CBM located at (0.00, 0.30, 0.33) 1/Å along the Γ -Z direction is about 380 meV (FIG. 3j). Moreover, a SO splitting of 109 meV is also observed at the absolute CBM which is located along the X-P direction. The SO splittings at the upper part of the VB at the N-, P- and Z-points are 28 meV, 106 meV, and 57 meV, respectively (FIG. 3b), and the maximum of the SO splitting reaches about 109 meV at (0.13, 0.13, 0.16) 1/Å along the X-P direction. The absolute size of the indirect band gap of Tl_{0.5}Li_{0.5}InSe₂, also depends on the SO interaction and we get $E_{\text{gap,WSO}}=2.18$ eV without and $E_{\text{gap,SO}}=2.07$ eV with SO interaction. Thus the transport properties of the Li-substituted compound Tl_{0.5}Li_{0.5}InSe₂ can be expected to be altered by the SO coupling which is in contrast to TlInSe₂ where the SO splitting does not affect electronic states near the gap.

E. Transport Properties

In order to quantitatively evaluate the electrical transport properties, the electrical conductivity σ , the electronic part of the thermal conductivity κ_e , and the Seebeck coefficient S have been calculated using the BoltzTraP code [31]. In general, wide-band gap materials have usually too small electrical conductivity to be considered as good thermoelectric materials. Here we investigate whether applying pressure or Li-doping are effective routes for improving the electrical conductivity in TlInSe_2 . The first approach results in the decrease of the band gap size while the second approach, i.e. substitution with smaller sized atoms, leads to a decrease of the effective mass. The temperature dependence of transport properties have been investigated for optimally p-doped TlInSe_2 at ambient pressure and at 20 GPa and for optimally p-doped $\text{Tl}_{0.5}\text{Li}_{0.5}\text{InSe}_2$ at ambient pressure. It should be noted that for the specific chemical potential the BoltzTraP code is given the temperature dependence of transport properties. Our DFT calculations based on the TB-mBJ functional yield a band gap closest to the available experimental data. Consequently, all calculations have been performed with the TB-mBJ functional. We evaluate the importance of the SO coupling for the transport properties by a comparative study of the macroscopic transport parameters obtained from DFT calculations with and without SO interaction. The melting point of TlInSe_2 is at $T=1040$ K [41], thus our calculations of the transport properties cover the temperature range from 40 K up to 1000 K.

Strictly speaking, the BoltzTraP code allows to calculate the electrical conductivity σ and the electronic thermal conductivity κ_e both divided by the relaxation time τ . In order to obtain the quantities σ and κ_e additional information on τ is thus required. Detailed calculations of wavevector-dependent relaxation times are beyond the scope of this work, instead we have chosen to use wavevector-independent approximations of the relaxation time. Two different approaches are

widely used in literature. The first one is a constant relaxation time approximation [42-43], where τ is simply assumed to be independent of temperature. Using experimental room temperature data for the electrical conductivity, the relaxation time is obtained from $\tau = \sigma_{\text{exp}} / (\sigma/\tau)_{\text{calc}}$. For TlInSe₂ at 300 K experimental values of $3.9 \times 10^{-2} \Omega^{-1}\text{m}^{-1}$ and $4.44 \times 10^{-2} \Omega^{-1}\text{m}^{-1}$ have been reported for the electrical conductivity along the c- and b-axes, respectively [44]. Using these values together with the results of our DFT calculations with the SO interaction for $(\sigma/\tau)_{\text{calc}}$ we obtain relaxation times τ of 7.71×10^{-12} s and 1.8×10^{-12} s along the c- and b-axes, respectively. Averaging over the three crystallographic directions we get $\tau = 3.79 \times 10^{-12}$ s for TlInSe₂.

A second, more realistic approach is to assume electron–phonon scattering as the dominating scattering process whereas neglecting scattering from ionized impurities and lattice imperfections. The scattering processes with phonons introduce a T-dependence whereas the impurity and defect scattering processes are expected to dominate only at low temperatures and are thus irrelevant at the elevated temperature range investigated here. We emphasize that we assume an isotropic relaxation time. A further refinement may take anisotropic scattering rates into account which is suggested by the anisotropic electron and phonon dispersions, however, this is beyond the scope of this work. The relaxation time is approximated by $\tau = CT^{-1}n^{-1/3}$ [45] where C is a constant, T is the temperature and n is the charge carrier concentration. In order to determine C we use T=300 K, the average relaxation time $\tau = 3.79 \times 10^{-12}$ s and the carrier concentration n which corresponds to the doping level matching the experimental Hall coefficient $R_{\text{H,exp}} = 21.9 \text{ m}^3\text{C}^{-1}$ of TlInSe₂ reported in Ref. [44]. We calculate $n_{\text{exp}} = 1/(e R_{\text{H,exp}})$ from the experimental Hall coefficient $R_{\text{H,exp}}$ (e is the electronic charge) which yields $n_{\text{exp}} = 2.93 \times 10^{11} \text{ cm}^{-3}$. $(\sigma/\tau)_{\text{calc}}$ is calculated using the BoltzTraP code with a chemical potential μ chosen to give the appropriate charge carrier concentration $n = n_{\text{exp}}$, where n is also calculated from R_{H} as determined by the BoltzTraP code. The constant is then given by $C = T n^{1/3} \sigma_{\text{exp}} / (\sigma/\tau)_{\text{calc}}$ at T=300K. This gives a value of $C = 7.55 \times 10^{-6} \text{ sKcm}^{-1}$. The relaxation time at

different temperatures and doping levels is then calculated from the above equation. We assume that the same constant $C=7.55\times 10^{-6}$ sKcm⁻¹ applies to the Li-substituted compound $\text{Tl}_{0.5}\text{Li}_{0.5}\text{InSe}_2$ keeping the dependence of the relaxation time on temperature and charge carrier concentration.

In the following, the results are presented with both approximations of the relaxation time each corresponding to the optimized p-type charge carrier concentration which gives the maximum power factor $S^2\sigma$ at 300 K for the investigated compounds. For the DFT calculation with the SO, we obtain carrier concentrations between 4.81×10^{17} cm⁻³ (at 40 K) and 5.21×10^{19} cm⁻³ (1000 K) for TlInSe_2 whereas carrier concentrations between 9.40×10^{18} cm⁻³ and 5.95×10^{20} cm⁻³ are found for $\text{Tl}_{0.5}\text{Li}_{0.5}\text{InSe}_2$ at 40 K and 1000 K, respectively.

FIG. 4 shows the transport properties of TlInSe_2 (red and blue lines) and $\text{Tl}_{0.5}\text{Li}_{0.5}\text{InSe}_2$ (green and brown lines) calculated with the SO and without the SO interaction. The upper right and left panels (FIG. 4a-f) correspond to the constant and the T- and n-dependent relaxation time approximation, respectively. FIG. 4g and h show the Seebeck coefficient S and the electronic figure of merit $(ZT)_e = S^2\sigma T/\kappa_e$ for which the relaxation time is not playing any role. We note that with this definition of $(ZT)_e$ the lattice thermal conductivity is not considered.

Clearly, the results for the electronic transport properties strongly depend on which approximation is used for the relaxation time. In case of TlInSe_2 the calculation with the SO and WSO interaction yield almost identical results whereas this is not the case for $\text{Tl}_{0.5}\text{Li}_{0.5}\text{InSe}_2$. This means that the SO coupling does alter the transport properties of $\text{Tl}_{0.5}\text{Li}_{0.5}\text{InSe}_2$, but SO interaction is not important for transport in TlInSe_2 . As discussed above, in $\text{Tl}_{0.5}\text{Li}_{0.5}\text{InSe}_2$ the SO splitting modifies the electronic states at the upper part of the VB at the Z-, P- and N-points (FIG. 3b) leading to a decrease of σ and κ_e , S. Overall these modifications of the bandstructure lead to a significant lowering of the power

factor. Finally, $(ZT)_e$ is reduced when the SO interaction is taken into account albeit in part compensated by the lower electronic thermal conductivity κ_e .

The electronic thermal conductivity κ_e for the constant and the T-/n-dependent approximation for the relaxation time are presented in FIG. 4a and b, respectively. For both cases κ_e continuously increases in the temperature interval from 40 K to 1000 K due to the increasing number of thermally excited charge carriers. With the constant relaxation time approximation (FIG. 4a) applied to TlInSe₂ the electronic thermal conductivity κ_e increases from 6.02 W/m-K (6.11 W/m-K) at 40 K by two orders of magnitude to 932 W/m-K (943 W/m-K) at 1000 K for calculations with the SO (WSO) interaction. With electron-phonon scattering the corresponding values are 0.102 W/m-K (0.103 W/m-K) and 0.423 W/m-K (0.426 W/m-K), respectively (FIG. 4b). Similarly, with a constant relaxation time the electronic thermal conductivity κ_e of Tl_{0.5}Li_{0.5}InSe₂ is 104 W/m-K (147 W/m-K) at 40 K increasing to 5175 W/m-K (6764 W/m-K) at 1000 K for calculations with the SO (WSO) interaction. However, with the T-/n-dependence of τ (FIG. 4b) significantly lower values of 0.238 W/m-K (0.334 W/m-K) and 0.466 W/m-K (0.609 W/m-K) are obtained. The change of the thermal conductivity κ_e due to the SO interaction is significant for the Li-substituted compound as qualitatively expected from the band structure behavior upon switching on the SO coupling. At elevated temperatures κ_e almost reaches a plateau since scattering is becoming increasingly important.

FIG. 4c shows that for optimally p-doped TlInSe₂ and constant relaxation time the electrical conductivity σ increases from 6.05×10^6 1/Ωm (6.18×10^6 1/Ωm) at 40 K to 1.66×10^7 /Ωm (1.68×10^7 1/Ωm) at 1000 K for calculations with the SO (WSO) interaction. This increase in σ reflects essentially the increase in charge carrier concentration. When considering electron-phonon scattering the electrical conductivity σ decreases with the 1/T behavior due to the shortened carrier

lifetime at higher temperatures. FIG. 4d shows the drop in σ from 1.03×10^5 1/ Ωm (1.04×10^5 1/ Ωm) to 7.57×10^3 1/ Ωm (7.61×10^3 1/ Ωm). In $\text{Tl}_{0.5}\text{Li}_{0.5}\text{InSe}_2$ the corresponding values with constant relaxation time range from 1.06×10^8 1/ Ωm (1.50×10^8 1/ Ωm) at 40 K to 1.55×10^8 1/ Ωm (2.08×10^8 1/ Ωm) at 1000 K (FIG. 4c) displaying a smooth increase due to the larger band gap and a higher absolute conductivity due to the larger doping level. Assuming electron-phonon scattering the (1/T)-dependence is again adopted and the corresponding values are 2.40×10^5 1/ Ωms (3.43×10^5 1/ Ωms) at 40 K and 1.40×10^4 1/ Ωms (1.87×10^5 / Ωms) at 1000K (FIG. 4d).

The power factor (PF) is shown in FIG. 4e and f for the two approximations of the relaxation time. For the non-substituted compound TlInSe_2 with constant τ the PF increases linearly. The SO coupling has no effect on the PF. A broad maximum is observed when taking the T-dependence of electron-phonon scattering into account. The maximum PF of 3.22×10^{-4} W/m-K² is reached at 580 K. This value is comparable to the PF of state-of-the-art thermoelectric materials. For example, the PF of Cu_2Se reaches a maximum of 1.3×10^{-3} W/m-K² at T=1000 K, SnSe along the crystallographic b-axis has a PF= 1.0×10^{-3} W/m-K² [2]. In Li-substituted $\text{Tl}_{0.5}\text{Li}_{0.5}\text{InSe}_2$ the PF only reaches a maximum of 1.93×10^{-4} W/m-K² (2.62×10^{-4}) at 230 K (250 K) for calculations with SO (WSO) coupling (FIG. 4f). This reduction in the PF demonstrates that the electronic properties of $\text{Tl}_{0.5}\text{Li}_{0.5}\text{InSe}_2$ are less favorable with regard to thermoelectric applications. Hence, Li-substitution turns out not to be a suitable optimization strategy in terms of improving the electronic materials properties.

Finally, the Seebeck coefficient and $(ZT)_e$ are shown in FIG. 4g and FIG. 4h, respectively. In TlInSe_2 the Seebeck coefficient reaches a maximum of 2.01×10^{-4} V/K (2.00×10^{-4} V/K) at 1000 K for the calculations with the SO (WSO) interaction whereas the corresponding values for

$\text{Tl}_{0.5}\text{Li}_{0.5}\text{InSe}_2$ are 7.28×10^{-5} V/K (8.60×10^{-5} V/K) at 1000 K. In Ref. [5] experimental data of the temperature dependence of the Seebeck coefficient in the range 423K-773 K for TlInSe_2 has been presented. This data shows a change of sign of the Seebeck coefficient to negative values when increasing the temperature with a crossover at around 473 K whereas such a behavior is absent in our data (FIG. 4g). Moreover, the experimental data in Ref. [5] reveals a large scatter of values for the Seebeck coefficient in the range 10^4 $\mu\text{V/K}$ to 10^7 $\mu\text{V/K}$ for temperatures from 273 to 423 K, presumably at much lower carrier concentration than we investigate here, which renders a comparison to our numerical data difficult. The maximum of $(ZT)_e$ is found in TlInSe_2 which is 0.72 at 1000 K. This value is quite close to the figure of merit ZT of state-of-the-art thermoelectric materials, e.g. $ZT = 1.6$ for Cu_2Se and $ZT=2.5$ for SnSe along the crystallographic b-axis. However, $(ZT)_e$ can only be considered as an upper limit to ZT as it does not include the lattice thermal conductivity [2]. A significantly lower $(ZT)_e$ is obtained for $\text{Tl}_{0.5}\text{Li}_{0.5}\text{InSe}_2$ where it only reaches 0.18 for calculations with the SO interaction.

The thermal conductivity κ_e , electrical conductivity σ , power factor, Seebeck coefficient S , and $(ZT)_e$ of TlInSe_2 at 20 GPa with the SO and WSO interaction are shown in FIG. 5a-d. For comparison the data at ambient pressure with the SO is also presented. In the constant- τ approximation the electronic thermal conductivity κ_e with the SO (WSO) is continuously increasing from 12.25 W/m-K (5.60 W/m-K) at 40 K to 1537 W/m-K (973.6 W/m-K) at 1000 K whereas the corresponding values for the T-/n-dependent approximation for τ are 0.18 W/m-K (0.11 W/m-K) and 0.85 W/m-K (0.54 W/m-K), respectively. Moreover, at 20 GPa the electronic thermal conductivity κ_e is substantially larger than at ambient pressure over the whole temperature range.

FIG. 5c-d shows that the electrical conductivity σ of TlInSe_2 at 20 GPa is larger as compared to ambient pressure conditions. As discussed above the lowest band gap (18 meV) is observed at 20 GPa when the SO interaction is taken into account. This drastic reduction of the band gap

significantly increases the thermally excited charge carrier concentration. Thus, the electrical conductivity is significantly higher than the electrical conductivity of TlInSe₂ at ambient pressure. Moreover, significant changes in the transport properties of TlInSe₂ close to the semiconductor-metal transition at 20 GPa are observed. This is also in line with the modifications of the bandstructure in terms of DOS and band gap (FIG. 2). The 1/T dependence from the scattering processes again dominates the temperature-dependent decrease of σ . The power factor at 20 GPa is significantly smaller compared to ambient pressure such that its maximum with the SO reaches only 16.47×10^{-2} W/m-K² at 510 K (constant τ) and 22.44×10^{-5} W/m-K² at 360 K (T/n-dependent τ).

The Seebeck coefficient is shown in FIG. 5g which reaches a maximum of 10.44×10^{-5} V/K (17.94×10^{-5} V/K) at 460 K (730 K) for the calculation with the SO (WSO) interaction. The $(ZT)_e$ of TlInSe₂ as shown in FIG. 5h is also smaller at 20 GPa compared to ambient pressure such with a maximum of 0.3 (0.61) at 390 K (600 K) for calculation with the SO (WSO) interaction. Although pressure significantly changes the band structure, the modifications result in less favorable transport properties for thermoelectric applications. We emphasize that our results are obtained at optimized Fermi level and thus optimized charge carrier concentration. This is an important difference to experimental work which typically investigates the modification of transport properties which pressure at constant doping concentration.

IV. CONCLUSION

In conclusion, the electronic structure and electronic transport properties of TlInSe₂ (at ambient pressure and 20 GPa) and the Li-substituted compound Tl_{0.5}Li_{0.5}InSe₂ have been calculated based on DFT and Boltzmann transport theory. We have used various functionals including the PBE functional, the TB-mBJ functional with the SO and without SO interaction as well as the B3LYP hybrid functional without the SO interaction. Our data (without SO interaction) reveals that the best

match of the band gap with the experimental data is obtained with the TB-mBJ functional whereas the gap size is significantly underestimated using the PBE functional. Moreover, our calculations identify TlInSe₂ as a direct band gap semiconductor up to pressures of 20 GPa. However, a second VBM and a second CBM are located at the Z-point. Compared to the VBM (CBM) at the M-point the second maximum (minimum) is only tens of meV lower (higher) in energy. In contrast, the Li-substituted compound Tl_{0.5}Li_{0.5}InSe₂ is an indirect band gap semiconductor. Three almost degenerate VBM are present within the volume of the BZ enhancing the electronic DOS close to the energy gap. Orbital band character analysis shows that the contributions of Se-p_y and Tl-s states dominate the electronic states at the VBM. The SO splittings (TB-mBJ) of bands have been observed at the Γ (354 meV), M (170 meV) and Z (141 meV) points of the BZ well inside the VB. In contrast, in Li-substituted Tl_{0.5}Li_{0.5}InSe₂ the SO splittings occur at the upper part of the VB at the Z-, P- and N-points and are 57 meV, 106 meV, and 28 meV, respectively. Our results of the transport properties of TlInSe and Tl_{0.5}Li_{0.5}InSe₂ reveal that the SO interaction plays a negligible role for the TE properties of TlInSe₂ but is significant for Tl_{0.5}Li_{0.5}InSe₂. When applying pressure in the range 0-30 GPa an increase of the VB width and a rigid shift of the CB to the lower energies are induced. Increasing the pressure leads to the closing of gap, and the compound shows metallic properties above 20 GPa.

Substitution of Li into the TlInSe₂ compound leads to a lower Seebeck coefficient and lower power factor as well as lower $(ZT)_e$. Hence Li-substitution does not lead to enhanced transport properties with respect to TE applications. In addition, increasing the pressure to 20 GPa which is close to the metallic transition temperature will not improve the Seebeck coefficient, the power factor and $(ZT)_e$ of TlInSe₂. This study thus identifies TlInSe₂ at ambient pressure with the most favorable electronic band structure for TE applications superior to both, TlInSe₂ under pressure with a lower band gap and Tl_{0.5}Li_{0.5}InSe₂ with a larger band gap.

References

- [1] Snyder G J and Toberer E S 2008 Nat. Materials **7** 105
- [2] Zhang X and Zhao L D 2015 J. of Materiomics **1** 92
- [3] Balandin A, Wang K L 1998 J. Appl. Phys. **84** 6149
- [4] Hicks L D, Dresselhaus M S 1993 Phys. Rev. B **47** 12727
- [5] Mamedov N, Wakita K, Ashida A, Matsui T, Morii K 2006 Thin Solid Films **499** 275
- [6] Müller D, Eulenberger G 1973 Z. Anorg, Allg. Chem. **398** 207
- [7] Chen X, Weathers A, Carrete J, Mukhopadhyay S, Delaire O, Stewart D A, Mingo N, Girard S N, Ma J, Abernathy D L, Yan J, Sheshka R, Sellan D P, Meng F, Jin S, Zhou J, Shi L 2015 Nat. Commu **6** 6723
- [8] Heremans J P, Jovovic V, Toberer E S, Saramat A, Kurosaki K, Charoenphakdee A, Yamanaka S, Snyder G J 2008 Science **321** 554
- [9] Pei Y, Shi X, LaLonde A, Wang H, Chen L, Snyder G 2011 Nature **473** 66
- [10] Alekperov O Z, Alianov M A, Kerimova E M 1998 J. Phys. **22** 1053
- [11] Gashimzade F M, Orudzhev G S 1980 Dokl. Akad. Nauk Azerb. SSR **36** 18
- [12] Orudzhev G, Mamedov N, Uchiki H, Yamamoto N, Iida S, Toyota H, Gojaev E, Hashimzade F 2003 J. Phys. Chem. Solids **64** 1703
- [13] Kohn W, Sham L J 1965 Phys. Rev. **140** A1133
- [14] Perdew J P 1986 Int. J. Quantum Chem. Symp. **19** 497
- [15] Mori-Sánchez P, Cohen A J, Yang W 2008 Phys. Rev. Lett. **100** 146401
- [16] Tran F, Blaha P 2009 Phys. Rev. Lett. **102** 226401
- [17] Becke A D, Johnson E R 2006 J. Chem. Phys. **124** 221101
- [18] Becke A D 1993 J. Chem. Phys. **98** 5648
- [19] Perdew J P, Burke K, Ernzerhof M 1996 Phys. Rev. Lett. **77** 3865
- [20] Zhang Y, Hao S, Zhao L, Wolverton C, Zeng Z 2016 J. Mater. Chem. A **4** 12073

- [21] Morozova N V, Ovsyannikov S V, Korobeinikov I V, Karkin A E, Takarabe K, Mori Y, Nakamura S, Shchennikov V V 2014 J. Appl. Phys. **115** 213705
- [22] Rabinal M K, Titus S S K, Asokan S, Gopal E S R, Godzaev M O, Mamedov N T 1993 Phys. Status Solidi B **178** 403
- [23] Weise S, Nowak E, Lenz A, Schumann B, Krämer V 1996 J. of Crystal Growth **166** 718
- [24] Hantias M, Anagnostopoulos A N, Kambas K, Spyridelis J 1989 Physica B **160** 154
- [25] Fan H Y 1956 Rep. Progr. Phys. **19** 107
- [26] Vijayakumar P, Magesh M, Arunkumar A, Anandha Babu G, Ramasamy P, Abhaya S 2014 J. of Crystal Growth **388** 17
- [27] Ma T, Zhu C, Lei Z, Yang C, Sun L, Zhang H 2015 J. of Crystal Growth **415** 132
- [28] Mitaray S, Kühn G, Schumann B, Tempel A 1986 Thin Solid Films **135** 251
- [29] Blaha P, Schwarz K, Madsen G, Kvaniscka D and Luitz J 2001 *Wien2k, An Augmented Plane Wave Plus Local Orbitals Program for Calculating Crystal Properties* (Vienna: Vienna University of Technology)
- [30] Wu Z, Cohen R E 2006 Phys. Rev. B **73** 235116
- [31] Madsen G K H, Singh D 2006 Com. Phys. Commu. **175** 67
- [32] Ghafari A, Boochani A, Janowitz C, Manzke R 2011 Phys. Rev. B **84** 125205
- [33] Ghafari A, Janowitz C, Manzke R 2013 Condens. Matter **25** 315502
- [34] Moustafa M, Ghafari A, Paulheim A, Janowitz C, Manzke R 2013 J. of Elec. Spec. and Related Phenomena **189** 35
- [35] Zeier W G, Zevalkink A, Gibbs Z M, Hautier G, Kanatzidis M G, Snyder G 2016 Angew Chem Int Ed Engl **55** 6826
- [36] Wang H, Pei Y, LaLonde A D, Snyder G J 2013 Thermoelectr. Nano mater. Springer Ser. Mater. Sci. 182 (Eds.: Koumoto K, Mori T), Springer Berlin pp. 3- 32
- [37] Kilday D G, Niles D W, Margaritondo G, Levy F 1987 Phys. Rev. B **35** 660

- [38] Li Guodong, Aydemir U, Morozov S I, Wood M, An Q, Zhai P, Zhang Q, Goddard W A, and Snyder G J, 2017 Phys. Rev. Lett. **119** 085501
- [39] Birch F 1947 Phys. Rev. **71** 809
- [40] Kosobutsky A V, Basalaev Y M 2014 Solid State Communications **199** 17
- [41] Asadov M M, Mustafaeva S N, Mamedov A N, Tagiyev D B 2015 Inorg. Materials **51** 1232
- [42] Kutorasinski K, Wiendlocha B, Kaprzyk S, Tobola J 2015 Phys. Rev. B **91** 205201
- [43] Hong A J, Li L, Zhu H X, Yan Z B, Liu J–M, Ren Z F 2015 J. Mater. Chem. A **3** 13365
- [44] Ebnalwaled A A, Al-Orainy R H 2013 Appl. Phys. A **112** 955
- [45] Yumnam G, Pandey T, Singh A K 2015 J. of Chemical Phys. **143** 234704

Table 1: Comparison of the direct band gap energies $E_{\text{gap, M}}$ at the M-point, $E_{\text{gap, Z}}$ at the Z-point and the indirect band gap energy $E_{\text{gap, MZ}}$ across the M- and Z-points as calculated for TlInSe₂. The PBE functional and the TB-mBJ functional were both used with spin-orbit coupling (SO) and without spin-orbit coupling (WSO). Calculations using the B3LYP hybrid functional do not include SO coupling. The SO splittings $\Delta_{\text{SO-}\Gamma}$, $\Delta_{\text{SO-M}}$, $\Delta_{\text{SO-Z}}$ refer to the Γ -, M- and Z-point, respectively. The gap energies for various hydrostatic pressures in the range 0-30 GPa were calculated with the TB-mBJ functional. All energies are given in eV. For comparison the range of experimental values for the band gaps reported in literature [22, 24-25] are also presented.

	direct gap				indirect gap		$\Delta_{\text{SO-}\Gamma}$	$\Delta_{\text{SO-M}}$	$\Delta_{\text{SO-Z}}$
Experiment	1.27-1.44				1.07-1.21				
Theory	WSO		SO		WSO	SO			
	$E_{\text{gap, M}}$	$E_{\text{gap, Z}}$	$E_{\text{gap, M}}$	$E_{\text{gap, Z}}$	$E_{\text{gap, MZ}}$				
PBE	0.41	0.58	0.21	0.38	0.54	0.34	0.40	0.18	0.17
B3LYP	0.97	1.11	-	-	1.04	-	-	-	-
TB-mBJ	1.06	1.21	0.83	0.98	1.17	0.94	0.354	0.17	0.14
TB-mBJ - 2 GPa	0.89	1.02	0.64	0.78	1.03	0.78	0.355	0.17	0.15
TB-mBJ - 5 GPa	0.78	0.97	0.55	0.73	0.93	0.69	0.363	0.17	0.15
TB-mBJ - 10 GPa	0.57	0.79	0.33	0.54	0.74	0.49	0.369	0.17	0.15
TB-mBJ - 15 GPa	0.40	0.65	0.15	0.38	0.59	0.33	0.373	0.13	0.05
TB-mBJ - 20 GPa	0.26	0.52	0.02	0.25	0.46	0.19	0.378	0.01	0.07
TB-mBJ - 25 GPa	0.13	0.42	0.13	0.13	0.35	0.19	0.383	0.11	0.18
TB-mBJ - 30 GPa	0.02	0.32	0.24	0.03	0.25	0.19	0.389	0.22	0.28

Table 2: Effective masses (in units of the free electron mass m_0) along the crystallographic a, b, and c directions at the VBM and the CBM, both at the M-point. For TlInSe₂ calculated values are based on the TB-mBJ functional with and without SO interaction while for Tl_{0.5}Li_{0.5}InSe₂ the values are based on the TB-mBJ functional with SO.

compound		VBM					CBM				
		m_a^*	m_b^*	m_c^*	m_I^*	m_{DOS}^*	m_a^*	m_b^*	m_c^*	m_I^*	m_{DOS}^*
TlInSe ₂	TB-mBJ+SO	0.31	0.31	1.76	0.43	0.55	0.50	0.50	0.65	0.54	0.55
	TB-mBJ	0.31	0.31	1.73	0.43	0.55	0.43	0.43	0.66	0.49	0.50
Tl _{0.5} Li _{0.5} InSe ₂		1.02	1.02	0.73	0.90	0.91	0.22	0.22	0.31	0.24	0.25

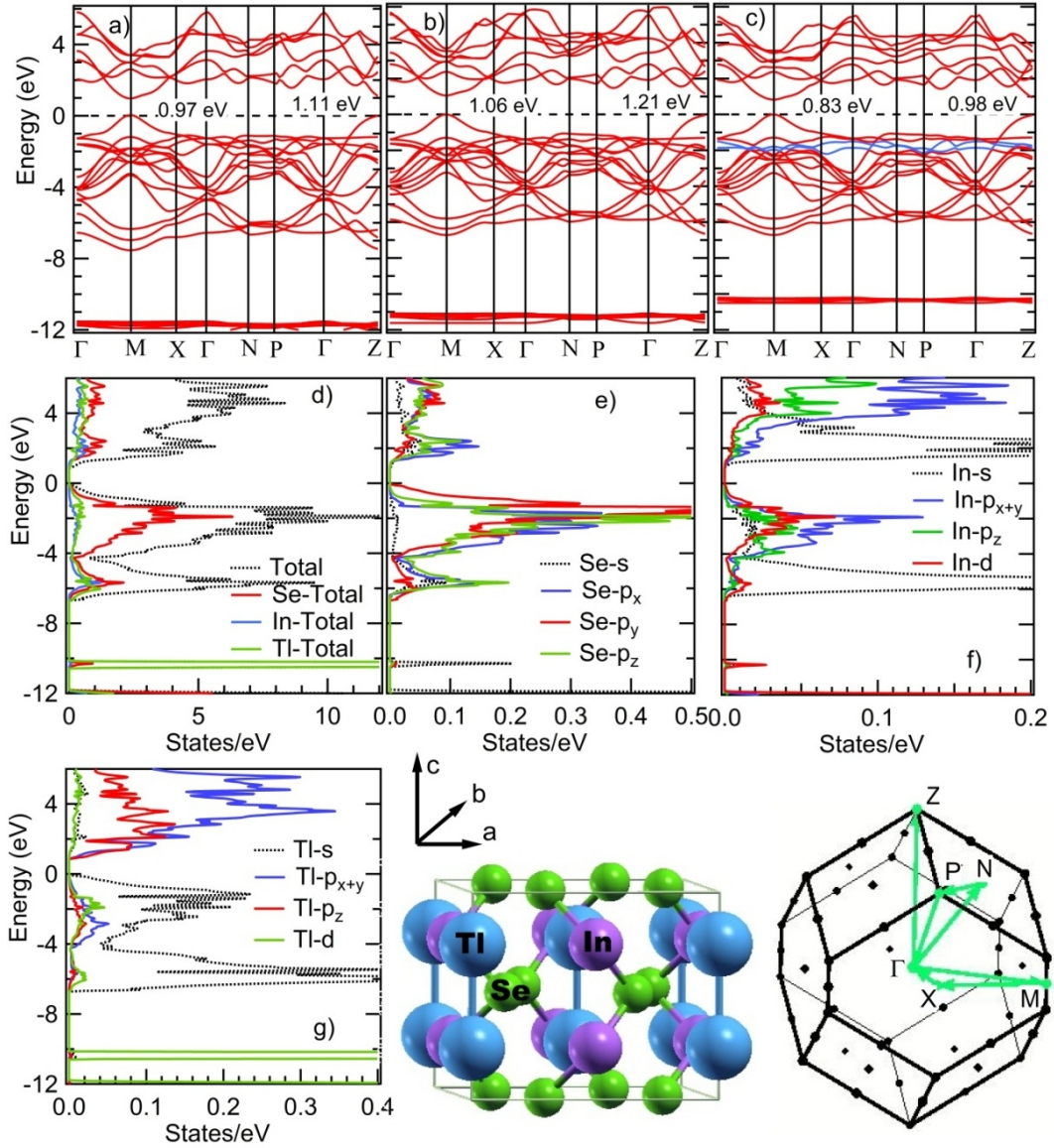


FIG. 1: Band structure of TIInSe_2 calculated using (a) the B3LYP hybrid functional; (b) the TB-mBJ functional without spin-orbit coupling and (c) the TB-mBJ functional with spin-orbit interaction. The two bands which show strong SO splitting are shown in blue color. In panels (a-c) the sizes of the direct gaps at the M- and at the Z-point are indicated as numerical values. Total DOS and partial DOS of TIInSe_2 as obtained with the TB-mBJ functional with SO interaction are shown in panels (d)-(g). The DOS values for the off-scale peaks dominated by TI-states at about -10 eV in panels (d) and (g) correspond to 82.4 states/eV and 41.2 states/eV, respectively. The crystal

structure and the Brillouin zone for space group $I4/mcm$ (140) with $c/a < 1$ are presented in the lower right panels.

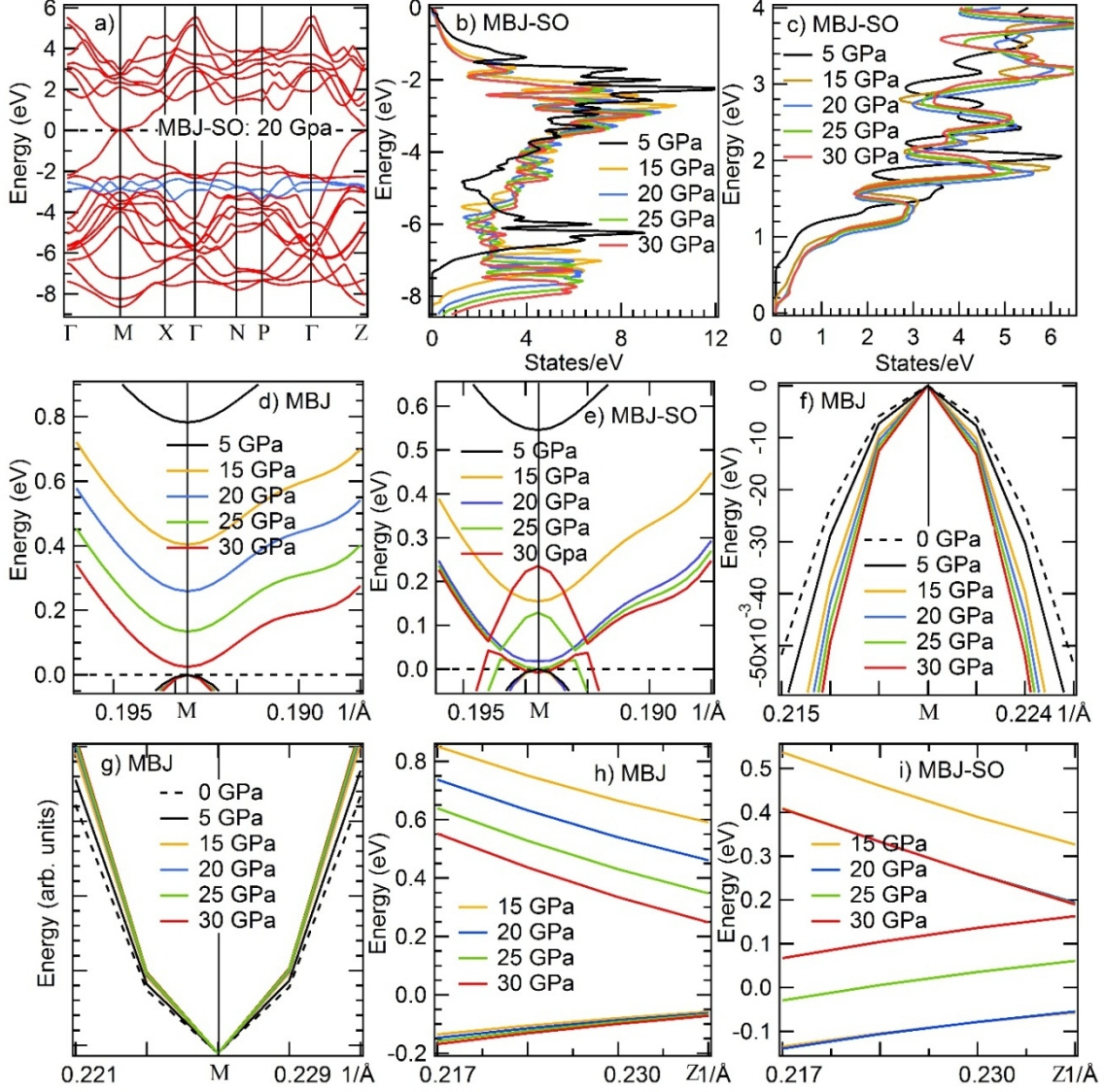


FIG. 2: (a) Band structure of TlInSe₂ at 20 GPa as obtained with the TB-mBJ functional with the SO interaction. The two bands which show strong SO splitting are shown in blue color. (b)-(c): Evolution of the DOS of TlInSe₂ with pressure in the range 0-30 GPa. Panels (d)-(e): Dispersion of the VBM and CBM at the M-point for pressures 5-30 GPa without and with the SO interaction. (f)-(g): Enlarged view of the dispersion region close to the VBM (panel f) and the CBM (panel g) at the M-point for pressures 0-30 GPa. (h)-(i): Dispersion of the VBM and CBM along the Γ -Z direction close to the Z-point for pressures 15-30 GPa without (panel h) and with SO interaction (panel i).

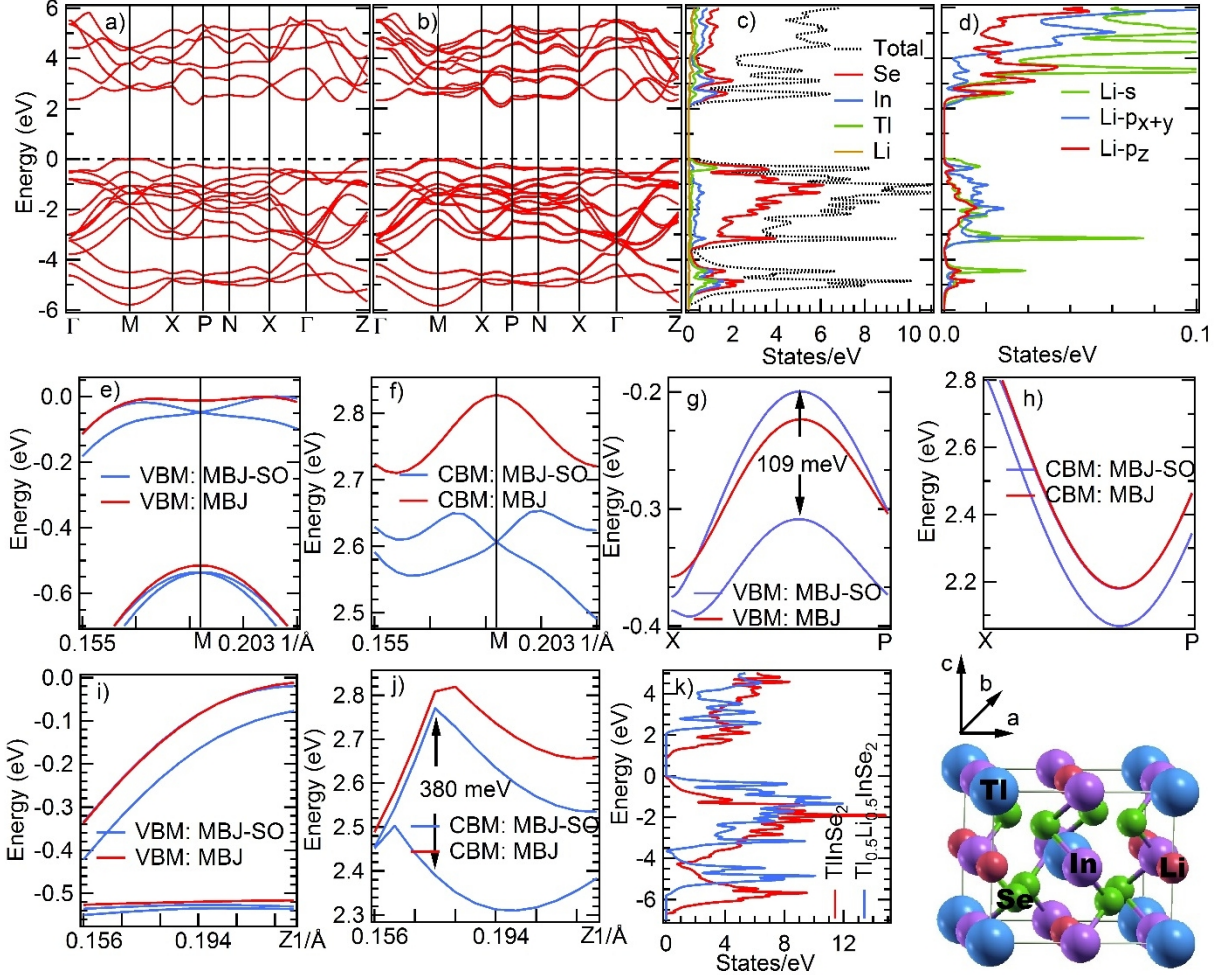


FIG. 3: (a) and (b) Band structure of $\text{Tl}_{0.5}\text{Li}_{0.5}\text{InSe}_2$ calculated with the TB-mBJ potential without and with the SO interaction. (c) Total and partial DOS of $\text{Tl}_{0.5}\text{Li}_{0.5}\text{InSe}_2$ calculated with the TB-mBJ potential with the SO interaction. (d) Partial DOS of the Lithium atom in the structure. (e)-(j) Zoom into the dispersion close to the top of the VBM and the bottom of the CBM at the M and Z-points as well as along the X-P direction of the BZ. (k) Comparison of the DOS for TlInSe_2 and $\text{Tl}_{0.5}\text{Li}_{0.5}\text{InSe}_2$ calculated with the TB-mBJ potential with the SO interaction. The crystal structure of $\text{Tl}_{0.5}\text{Li}_{0.5}\text{InSe}_2$ is shown in the bottom right panel.

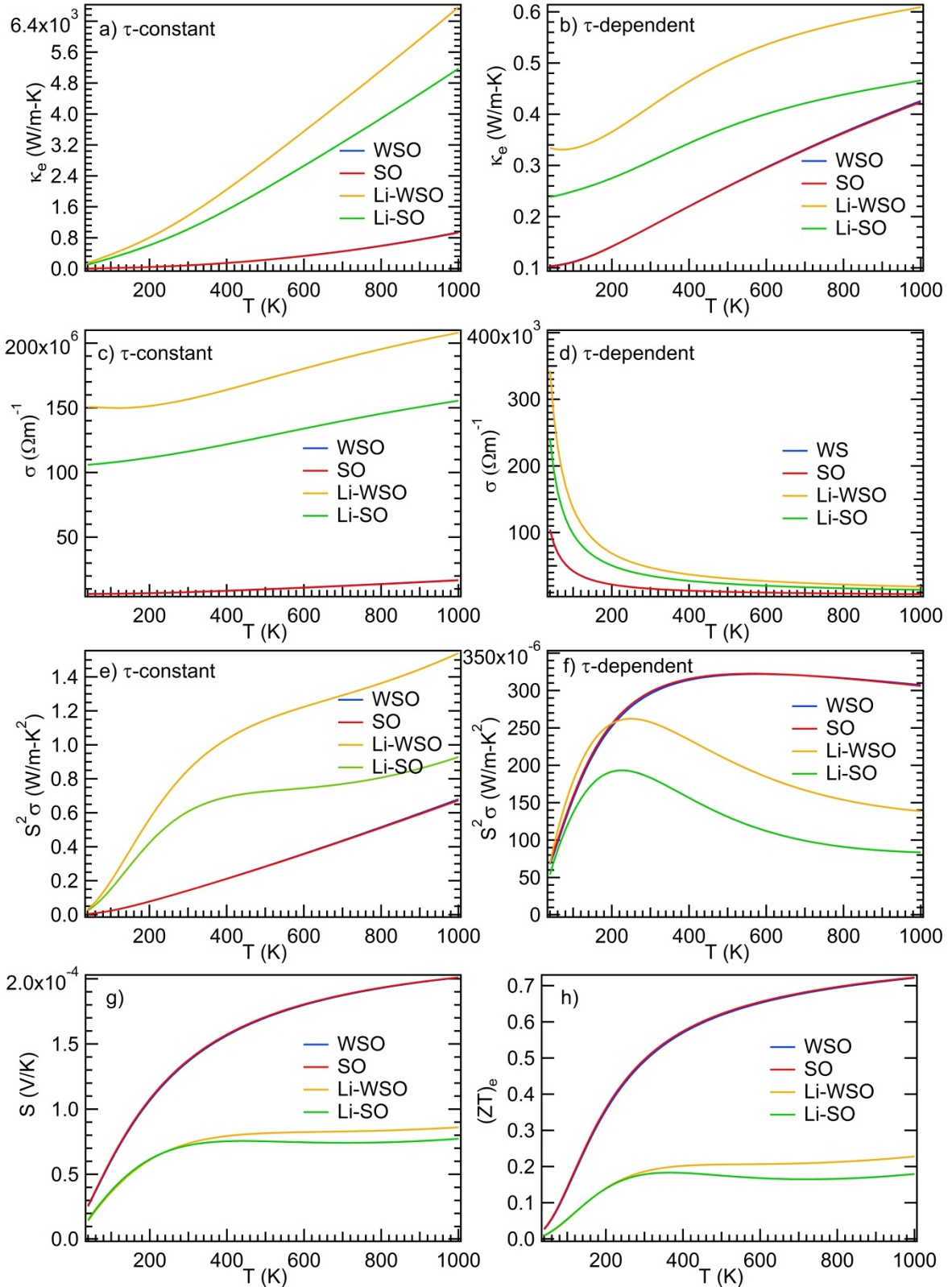


FIG. 4: (a)-(f): Calculated transport properties of TlInSe_2 (red and blue lines fall on top of each other) and of $\text{Tl}_{0.5}\text{Li}_{0.5}\text{InSe}_2$ (brown and green lines). The electronic part of the thermal conductivity κ_e , the electrical conductivity σ and the Seebeck coefficient S are given for the optimal doping level which maximizes the power factor. Panels (a), (c) and (e) on the left side show results for a constant relaxation time τ . Panels (b), (d) and (f) on the right side show results for a temperature- and charge carrier concentration dependent relaxation time τ (see text). Panels (g) and (h) show the Seebeck coefficient S and the electronic figure of merit $(ZT)_e$. The results presented with the SO and WSO interaction (line color indicated in the inset).

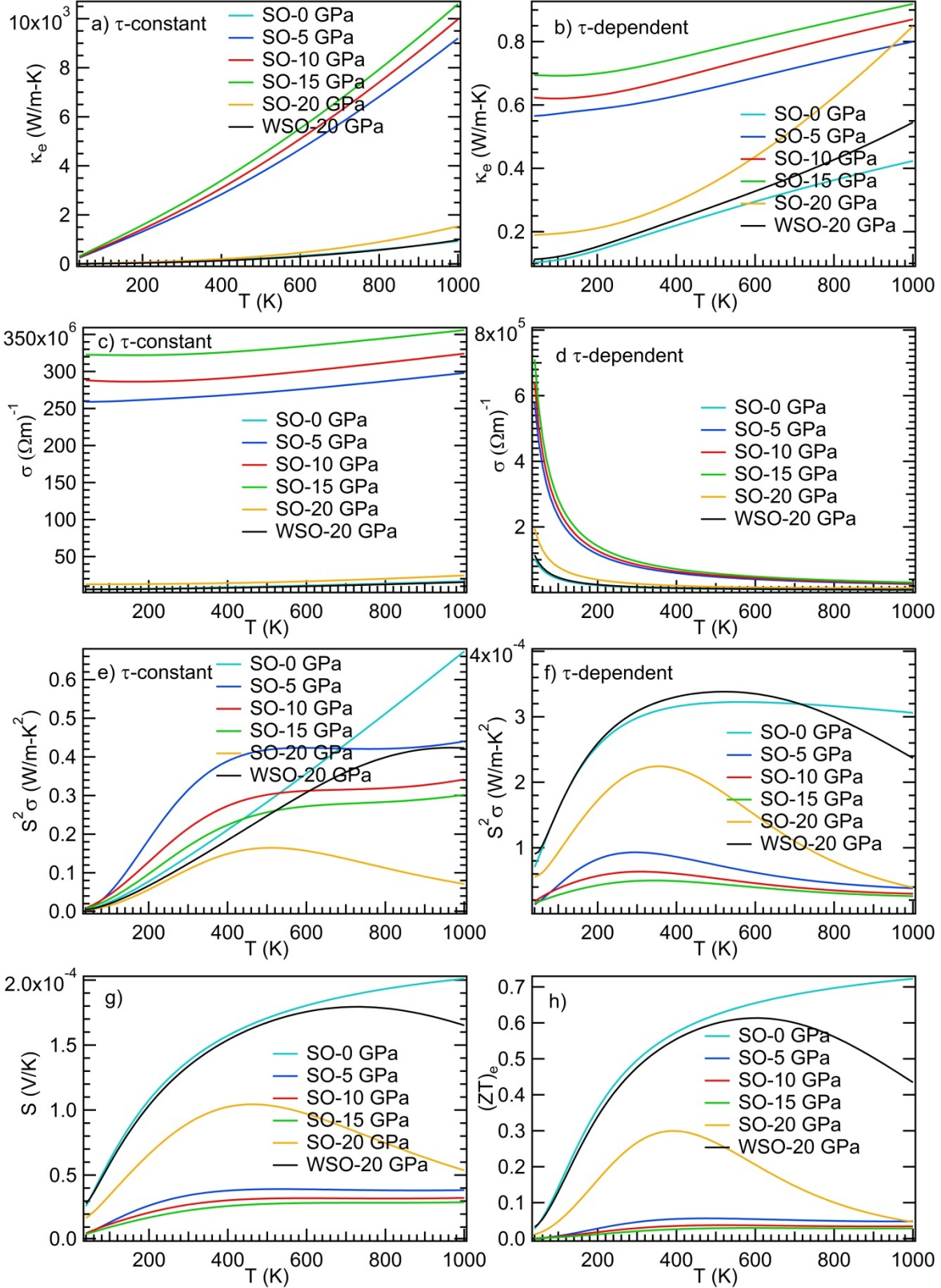


FIG. 5: (a)-(f): The transport properties of TlInSe_2 at 20 GPa with the SO interaction (brown lines) and WSO interaction (black lines). Data at ambient pressure (blue lines) are also shown for comparison. The electronic part of the thermal conductivity κ_e , the electrical conductivity σ and the

Seebeck coefficient S are given for the optimal doping level which maximizes the power factor. Panels (a), (c) and (e) on the left side show results for a constant relaxation time τ . Panels (b), (d) and (f) on the right side show results for a temperature- and charge carrier concentration dependent relaxation time τ (see text). Panels (g) and (h) show the Seebeck coefficient S and the electronic figure of merit $(ZT)_e$.